Exact BER Analysis of NOMA with Arbitrary Number of Users and Modulation Orders

Hamad Yahya, *Student Member, IEEE,* Emad Alsusa, *Senior Member, IEEE,* and Arafat Al-Dweik, *Senior Member, IEEE,*

Abstract

Non-orthogonal multiple access (NOMA) is considered a promising candidate for future mobile networks due to its ability to provide improved spectral-efficiency, massive connectivity and low latency. As such, studying the bit error rate (BER) performance of NOMA is crucial, particularly as its BER performance depends on the power assignment for each user. Therefore, this paper derives exact BER expressions under additive white Gaussian noise (AWGN) and Rayleigh fading channels for an arbitrary number of NOMA users, where each user employs quadrature amplitude modulation (QAM) with an arbitrary modulation order. Furthermore, the power coefficient bounds (PCB), which ensure fairness between users and solve the constellation points ambiguity problem, are derived for the two and three users NOMA system with arbitrary, but identical, modulation orders. However, the procedure to find these bounds for any modulation orders are exemplified. In addition, this paper finds the optimal power assignment that minimizes the system's average BER for $N = 2$ and 3 users cases. The integrity of the analytical expressions is verified by Monte Carlo simulations, where the results give a valuable insight on the system's BER performance and power assignment granularity. It is shown that the feasible power assignment range becomes significantly small as the modulation order, or the number of users, increases, where the BER performance degrades due to the increased inter-user interference (IUI).

Index Terms

Non-orthogonal multiple access (NOMA), bit error rater (BER), arbitrary number of users, arbitrary modulation order, quadrature amplitude modulation (QAM).

Hamad Yahya and Emad Alsusa are with the Department of Electrical and Electronic Engineering, The University of Manchester, Manchester, M13 9PL, UK. (email: hamad.mohamadaliyahya@manchester.ac.uk, e.alsusa@manchester.ac.uk)

Arafat Al-Dweik is with Center for Cyber Physical Systems (C2PS), Khalifa University, Abu Dhabi, P.O.Box 127788, UAE. He is also with the Department of Electrical and Computer Engineering, Western University, London, ON, Canada. (e-mail: dweik@fulbrightmail.org).

I. INTRODUCTION

Future wireless networks are envisioned to provide ubiquitous and unlimited wireless coverage, which require integrating space, air, ground, and underwater networks in one large multidimensional network architecture [1]. Recent advances in non-orthogonal multiple access (NOMA) has made it a promising candidate for future mobile networks because it provides improved spectral efficiency, massive connectivity and low latency [2]–[6]. To date, several articles have investigated applying NOMA in various network scenarios including the Internet of Things (IoT), satellite communication, unmanned aerial vehicle (UAV) communications, and underwater communication [7]–[12]. For instance, [7] studied NOMA for IoT networks to provide reliable secure short packet communication for downlink and uplink. In addition, [8], [9] investigated the NOMA application in forward link of multibeam satellite. A framework for UAVs serving ground users using NOMA is studied in [10]. The integration of NOMA with visible light communication (VLC) systems for indoor environments is discussed [11], and its performance is studied for underwater communications [12].

The widely considered power-domain NOMA, conventional NOMA (C-NOMA), is based on utilizing the power domain to multiplex different signals through superposition coding (SC), where distinct power coefficients are allocated to the users before combining their signals [13]. The absence of orthogonality between users' signals introduces inter-user interference (IUI), which makes it necessary for certain users to use multi-user detection schemes to be able extract their own signals at the receiver side [14]. The most common schemes for multi-user detection of NOMA signals are successive interference cancellation (SIC) and joint-multi-user maximum likelihood detector (JMLD) [15], [16].

Bit error rate (BER) analysis of NOMA has recently received increased attention in the literature where both imperfect and perfect SIC detectors as well as JMLD are taken in consideration [12], [15]–[26]. The first attempt to approximate the BER using derived symbol error rate (SER) expressions for the downlink direction is in [17], where two users are assumed with different modulation scheme combinations such as binary phase shift keying (BPSK) + BPSK, quadrature phase shift keying (QPSK) + BPSK and quadrature amplitude modulation (QAM) + QAM. Nonetheless, the SER analysis is for additive white Gaussian noise (AWGN) channel. Furthermore, the authors of [18] provided the exact closed-form BER expressions for an uplink two users NOMA system with QPSK modulation over AWGN channel where the uplink NOMA

model is assumed to be perfectly synchronized and imperfect SIC is considered at the base station. In [19] exact BER expressions are derived for VLC-NOMA system with arbitrary number of users employing on-off keying (OOK) where imperfect SIC and perfect channel state information (CSI) are assumed.

Moreover, the first paper to consider a fading wireless channel, i.e. a single-input-single-output (SISO) Rayleigh fading broadcast channel, is [20] where exact closed-form BER expressions are derived for downlink while approximate expressions are derived for uplink. It is worth mentioning that two users are considered only where the analysis is limited to the modulation scheme of QPSK for the near user and BPSK for the far user. The authors of [21] derived closed-form expressions for the union bound on the BER of downlink NOMA with imperfect SIC over Nakagami-m fading channels. These bounds show estimates of the BER rather than exact BER. On the other hand, Assaf *et. al.* found exact closed-form downlink BER expressions for imperfect SIC over SISO Nakagami-m flat fading channels in [22] where two and three users are considered with QPSK. In [23] closed-form BER expressions are derived for two users NOMA-VLC system in downlink considering M-ary phase shift keying (M-PSK), M-ary pulse amplitude modulation (M-PAM), and M-QAM. In addition, Alqahtani *et. al.* [24] derived exact closed-form BER expressions for two users case employing BPSK in flat fading channels that are modelled by $\alpha-\eta-\mu$ fading distribution to study the significance of different fading parameters on the BER performance, namely non-linearity (α), different power between signal's in-phase and quadrature components (η), and the amount of multipath clusters (μ). The considered channel model can be approximated to Rayleigh, Weibull, Nakagami-m, $\alpha-\eta$ and $\alpha-\mu$ fading channel models.

Furthermore, in [25] closed-form BER is derived for arbitrary number of users using BPSK under Rayleigh flat fading, where perfect and imperfect SIC are assumed. Also, they claim that they derived a feasible range for proper power assignment which ensures a good BER performance for each user. Assaf *et. al.* extended the work in [22] for two users system to arbitrary square quadrature modulation orders, where square QAM was considered and systematic BER expressions were derived [15]. Additionally, the proper power assignment was formulated to ensure fairness between the users and to avoid constellation points overlap. Nonetheless, the work was limited to two users case only, yet BPSK and 8-QAM modulation orders were not considered. In [12] exact closed-form BER expressions are derived for VLC-NOMA system consisting two users with OOK modulation in underwater environments. Furthermore, Assaf *et.*

al. proved that the analysis of SIC and JMLD lead to the same final expression under perfect and imperfect CSI [16].

Analytical SER expressions were derived for C-NOMA systems in [27]–[29]. The authors of [27] considered two users case in the downlink direction using arbitrary QAM, where imperfect SIC is assumed. In addition, the condition for proper power assignment was introduced by them for the first time considering two users case. The approximation of the BER using the SER was found to be inaccurate for high modulation order or at low signal-to-noie ratio (SNR) values [15]. Moreover, the authors of [28] considered a threshold detector rather than SIC. It is found that the analytical performance of the proposed detector is very close to the SIC detector. Nonetheless, at low SNR values the performance of the threshold detector is worse.

A. Motivation and Contribution

Having closed-form expressions for either BER or SER allows the system designer to find optimal power assignment that satisfies certain requirements. These requirements can be based on the closed-form expressions including other constraints such as transmission power [29]. Based on the aforementioned literature and to the best of the authors knowledge, no work has considered BER analysis for more than two NOMA users using arbitrary modulation order even though NOMA is meant to support massive connectivity [6]. Inspired by the above, this paper considers the performance analysis of an arbitrary number of NOMA users using arbitrary modulation orders including BPSK, QPSK and M-QAM for the first time in the literature. The main contributions of this paper can be summarized as follows:

- Derive closed-form BER expressions for C-NOMA in the downlink direction considering arbitrary number of users, N, with arbitrary modulation orders.
- Evaluate the BER for different power assignments and validate the integrity of the results using computer simulation.
- Develop a method to find the power coefficients' bounds (PCB) which solve the constellation points ambiguity problem for $N = 3$ case, where arbitrary modulation orders are considered. Also, closed-form PCB expressions for the identical modulation orders scenario are derived.
- Find the optimal power assignments that minimize the system's average BER for $N = 2$ and 3 cases considering the derived PCBs as linear and non-linear constraints.

B. Paper Organization

The rest of the paper is organized as follows. In Sec. II, the system and channel models are introduced. Then, with the aid of an example, the generalized BER expressions are derived in Sec. III for N NOMA users with arbitrary modulation orders. Sec. IV demonstrates the analysis of the PCB, while Sec. V presents analytical and Monte Carlo simulation results, as well as the optimal power assignments results. Finally, Sec. VI concludes the paper with a summary of the main findings.

II. System And Channel Models

In downlink C-NOMA, the base station multiplexes the information symbols of N users using the same radio resources by assigning each user a distinct power coefficient based on its channel conditions. Without loss of generality, we assume that the N users are ordered in ascending order of their channel envelope, i.e. $|H_1| > |H_2| > \cdots > |H_N|$, where H_n, $1 \leq n \leq N$, is the complex channel gain of the link between the base station and the nth user. Therefore, the power assignment is performed such that a user with severe fading conditions is assigned higher power than a user with good channel conditions [21], [22]. In such scenarios, the power coefficients $\{\alpha_1, \alpha_2, \ldots, \alpha_N\}$ are assigned such that $\alpha_1 < \alpha_2 < \cdots < \alpha_N$, where $\sum_{n=1}^{N} \alpha_n = 1$. Fig. 1 shows an illustrative diagram of the system model for a single cell. The SC process at the base station is described by

$$x_{SC} = \sum_{n=1}^{N} \sqrt{\alpha_n} x_n \tag{1}$$

where x_n is the information symbol of the nth user, which is drawn uniformly from M-QAM constellation χ_n. For QAM signals, the information symbols typically have $\mathbb{E}[x_n] = 0$ and $\mathbb{E}[|x_n|^2] = 1 \quad \forall n$, where $\mathbb{E}[\cdot]$ denotes the statistical expectation. Consequently, the average signal of the NOMA symbols is normalized to unity such that $\mathbb{E}[|x_{SC}|^2] = 1$. To exemplify the SC process, Fig. 2 shows the constellation diagram of the resultant NOMA symbols using $\boldsymbol{M} = [4, 4, 2]$, where $\boldsymbol{M}$ is a vector that comprises the users' modulation orders such that $\boldsymbol{M} = [M_1, M_2, \ldots, M_N]$. In addition Fig. 2a shows each users' constellation points scaled with its respective power coefficient, while Fig. 2b shows the NOMA constellation points for $N = 2$ when U_1 and U_2 are considered. Furthermore, Fig. 2c shows the NOMA constellation points for $N = 3$ which can be seen as the superposition coding of Fig. 2b NOMA constellation points, $N = 2$, with U_3 constellation points. The amplitudes shown in Fig. 2 can be determined by the

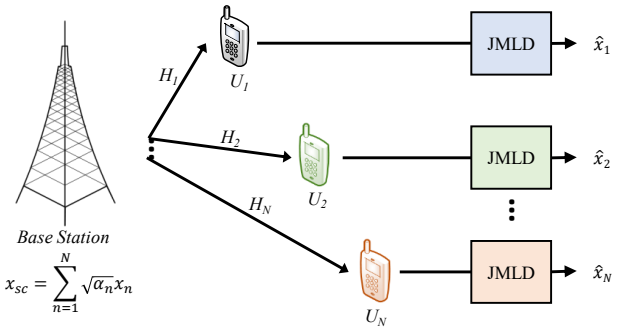

Fig. 1: Illustrative diagram of the system model assuming joint multiuser maximum likelihood detector (JMLD) at the receivers.

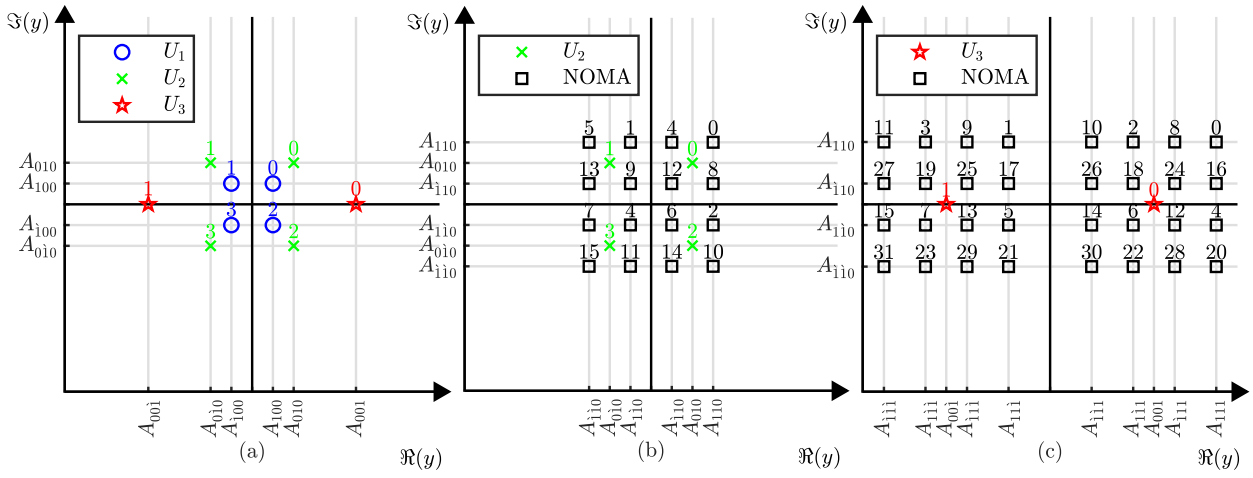

Fig. 2: Constellation points of: (a) All users without superposition coding. (b) U_2 and the superposition coding between U_1 and U_2. (c) U_3 and the superposition coding among U_1, U_2 and U_3.

following example, $A_{\grave{1}10} = -\frac{1}{\sqrt{2}} \times \sqrt{\alpha_1} + \frac{1}{\sqrt{2}} \times \sqrt{\alpha_2} + 0 \times \sqrt{\alpha_3}$, where the normalization factor, κ_n, for each user is included such that $\kappa_1 = \kappa_2 = 2$ and $\kappa_3 = 1$. Also, it can be noted that the NOMA word is stated as a decimal above each NOMA constellation point which corresponds to the users' bits. Taking the NOMA constellation points in Fig. 2c as an example, when converting the NOMA word decimal to a binary base, the leftmost two bits would belong to U_1, while the middle two bits belong to U_2 but the rightmost bit belongs to U_3. The amplitudes of the NOMA constellation points and the NOMA word can be easily extended to higher numbers of users, $N > 3$, as well as arbitrary modulation orders by following the same principle.

At the receiver front-end, the received baseband signal in flat fading channels is written as

$$y_n = H_n x_{SC} + W_n \tag{2}$$

where $W_n \sim \mathcal{CN}(0, \sigma^2_{W_n})$ is the AWGN, and $w_n = \Re[W_n] = \Im[W_n]$. In channels with small scale Rayleigh fading and large scale pathloss, the channel gain $H_n = \sqrt{\beta_n} \times h_n$, $h_n \sim \mathcal{CN}(0, \sigma^2_{h_n})$, $\beta_n = \Upsilon_n^{-\lambda}$, Υ_n is the distance between the base station and the nth user, and λ is the pathloss exponent. The small scale fading coefficients of different users are considered independent and identically distributed (i.i.d) random variables. Given that CSI is known perfectly at the receiver, the information symbols can be recovered using JMLD,

$$\{\widehat{x}_1, \widehat{x}_2, ..., \widehat{x}_N\} = \arg \min_{x_i \in \chi_i} \left| y_n - H_n \sum_{i=1}^{N} \sqrt{\alpha_i} x_i \right|^2 \tag{3}$$

where $\{\widehat{x}_1, \widehat{x}_2, ..., \widehat{x}_N\}$ are the jointly detected N users' symbols, and x_i represents the trail symbols for the ith user which are taken from the codebook χ_i. It is noted that when perfect CSI is considered at the receiver, the performance of SIC and JMLD is identical [15], [16]. Therefore, JMLD is considered in this paper to have a more compact and systematic analysis.

III. Generalized BER Analysis

To simplify the BER analysis in this paper, the simple example shown in Fig. 2 is considered here as well, where $\boldsymbol{M} = [4, 4, 2]$. The analysis for this example is generic, where the same steps can be applied for arbitrary number of users and arbitrary modulation orders. In this section, the conditional BER expressions will be derived and then the unconditional BER expressions will be shown. To get the BER, all possible transmitted symbols must be considered. Nonetheless, when equally probable symbols are assumed, the BER can be calculated considering only the first quadrant in the space diagram due to symmetry.

The analysis of the conditional BER is based on the probability that a transmitted NOMA symbol leads to an erroneous received bit. Therefore, finding the decision regions for each bit is crucial. Once these decision regions are determined, the BER calculation for each transmitted symbol can be calculated by finding the Euclidean distance to the decision regions' boundaries.

A. Decision Regions' Boundaries

The first step to find the decision regions' boundaries is by mapping the NOMA constellation points vector, $\boldsymbol{p}$, to a scatter matrix $\boldsymbol{P}$ that maps the spatial position of each constellation point

Algorithm 1 NOMA constellation points mapping.

procedure CONSTELLMAP($\boldsymbol{p}$) ▷ Scatter matrix for $\boldsymbol{p}$
  $\boldsymbol{p}_{\Re} \leftarrow \text{sort}(\Re[\boldsymbol{p}], \text{“ascend”})$ ▷ Left to right
  $\boldsymbol{P}_{\Re} \leftarrow \text{reshape}(\boldsymbol{p}_{\Re}, [u, v])$
  $\boldsymbol{p}^{*}_{\Im} \leftarrow \text{sort}(\Im[\boldsymbol{p}], \text{“descend”})$ ▷ Top to bottom
  $\boldsymbol{p}^{**}_{\Im} \leftarrow \text{unique}(\boldsymbol{p}^{*}_{\Im})$
  $\boldsymbol{p}_{\Im} \leftarrow \text{reshape}(\boldsymbol{p}^{**}_{\Im}, [\text{u}, 1])$
  $\boldsymbol{P} \leftarrow \boldsymbol{P}_{\Re} + 1j \times \boldsymbol{p}_{\Im}$
  return $\boldsymbol{P}$
end procedure

Algorithm 2 NOMA word's kth bit mapping.

procedure BITSMAP($\boldsymbol{b}_k$, $\boldsymbol{p}$, $\boldsymbol{P}$) ▷ Scatter matrix for $\boldsymbol{b}_k$
  for $i = 1 : u$ **do**
    for $j = 1 : v$ **do**
      $B^{(k)}_{i,j} \leftarrow \arg\min_{x_i \in \chi_i} \left| P_{i,j} - \sum_{i=1}^{N} \sqrt{\alpha_i} x_i \right|^2$
    end for ▷ MLD to find the most likely bit
  end for
  return $\boldsymbol{B}_k$
end procedure

to the matrix indices as can be seen in Fig. 3, where $\boldsymbol{p} \in \mathbb{C}^{1\times 2^q}$, $q = \sum_{i=1}^{N} \log_2 M_i$, $\boldsymbol{P} \in \mathbb{C}^{u\times v}$, u is the number of the rows in the scatterplot, while v is the number of the columns. Similarly, each bit in the NOMA word, X, will have a scatter matrix $\boldsymbol{B}_k \in \mathbb{R}^{u\times v}$, where $1 \leq k \leq q$. The scatter matrix $\boldsymbol{B}_k$ is produced from the NOMA word's kth bit vector, $\boldsymbol{b}_k \in \mathbb{R}^{1\times 2^q}$, that stores the corresponding kth bit for the NOMA constellation points $\boldsymbol{p}$, where the spatial position of the kth bit is mapped to $\boldsymbol{B}_k$. The algorithms to produce the scatter matrices $\boldsymbol{P}$ and $\boldsymbol{B}_k$ are shown in Algorithm 1 and Algorithm 2, respectively.

Algorithm 1 is based on finding the real and imaginary voltage levels and re-creating the scatter matrix $\boldsymbol{P}$ by moving from left to right and top to bottom. Furthermore, Algorithm 2 is mainly based on the results from Algorithm 1, where MLD is used to find the kth bit for each constellation point in $\boldsymbol{P}$.

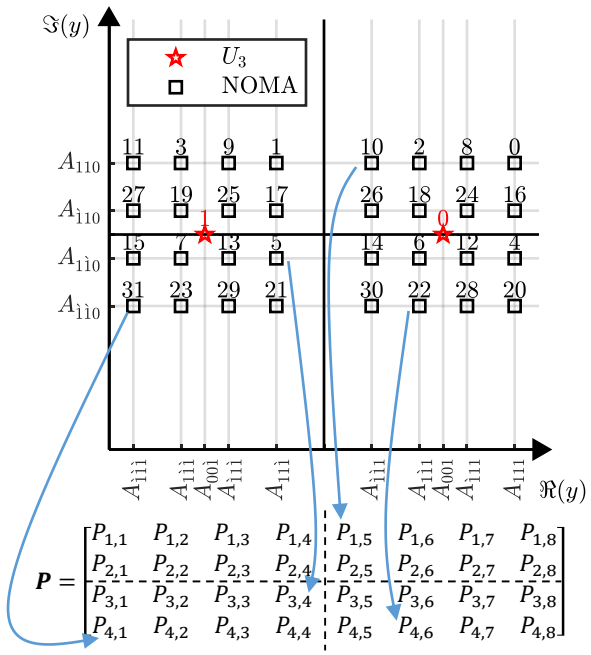

Fig. 3: Mapping NOMA constellation points to a scatter matrix $\boldsymbol{P}$ for $\boldsymbol{M} = [4, 4, 2]$

Now, since $\boldsymbol{P}$ is found, the real and imaginary primary decision regions' boundaries, $\boldsymbol{D}_l$, can be found by using a moving average filter with a window of size 2, where $l \in (\Re, \Im)$, $\boldsymbol{D}_\Re \in \mathbb{R}^{1\times u-1}$, $\boldsymbol{D}_\Im \in \mathbb{R}^{1\times v-1}$. This can be expressed as follows

$$D_U^{\Re} = \frac{1}{2}\Re\left[P_{1,U} + P_{1,U+1}\right] \tag{4}$$

and

$$D_V^{\Im} = \frac{1}{2}\Im\left[P_{V,1} + P_{V+1,1}\right] \tag{5}$$

where $U \in (1, u-1)$, $V \in (1, v-1)$. To find the decision regions' boundaries for the kth bit in the NOMA word, the scatter matrix $\boldsymbol{B}_k$ must be used, where the decision region boundary appears if there is a bit flip. Therefore, exclusive-or operator can be used over one row or one column of $\boldsymbol{B}_k$ to find the bit flip. This can be expressed as follows

$$T_{k_U}^{\Re} = B_{1,U}^{(k)} \oplus B_{1,U+1}^{(k)} \tag{6}$$

and

$$T_{k_V}^{\Im} = B_{V,1}^{(k)} \oplus B_{V+1,1}^{(k)} \tag{7}$$

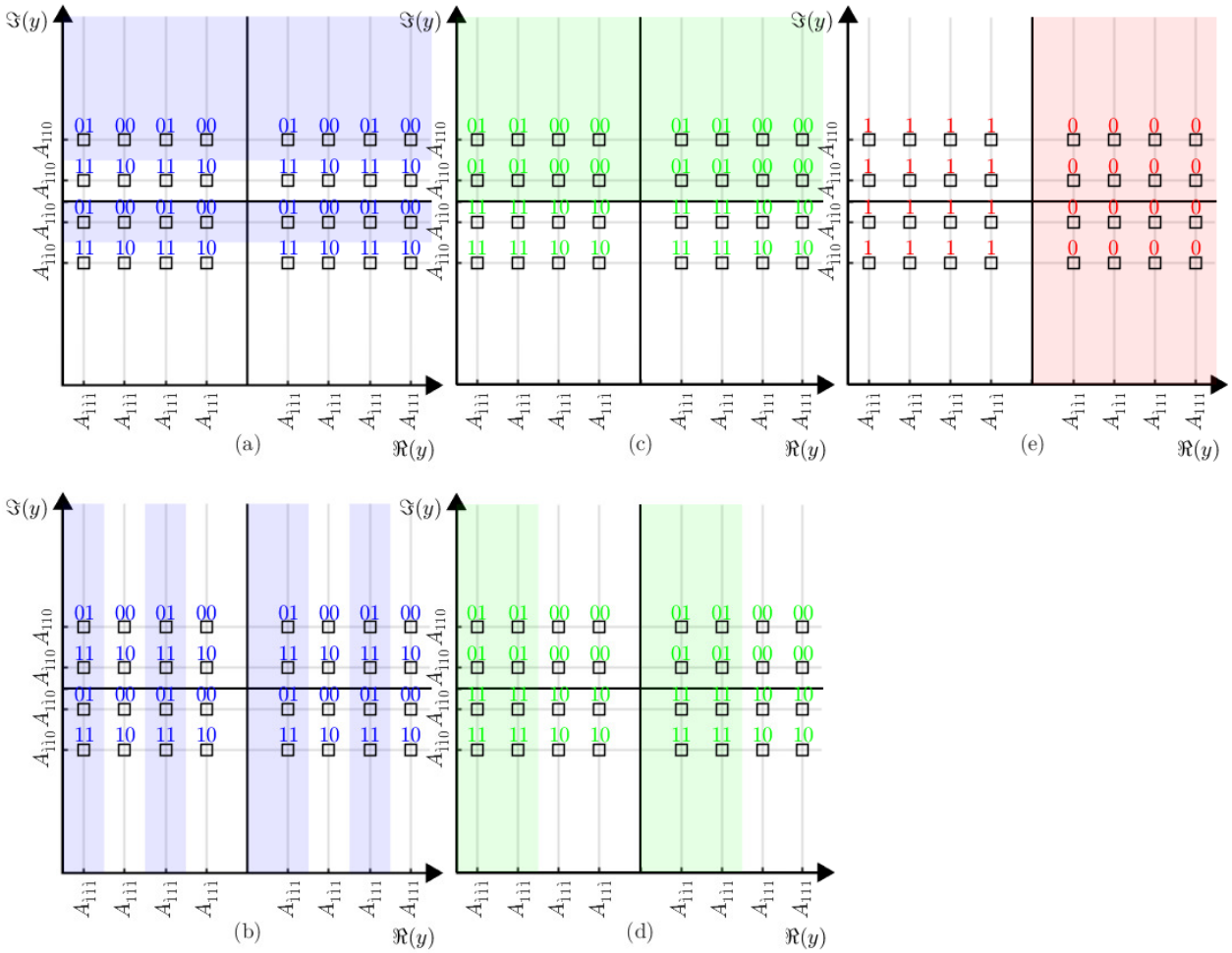

Fig. 4: NOMA constellation points for $\boldsymbol{M} = [4, 4, 2]$ showing the decision regions for: (a) first bit of U_1. (b) second bit of U_1. (c) first bit of U_2. (d) second bit of U_2. (e) U_3.

where $\boldsymbol{T}_k^{\Re} \in \mathbb{R}^{1\times u-1}$, $\boldsymbol{T}_k^{\Im} \in \mathbb{R}^{1\times v-1}$. By studying the constellation points in Fig. 2, it can be noted that the kth bit shows a bit flip, i.e. 1, in either $\boldsymbol{T}_k^{\Re}$ or $\boldsymbol{T}_k^{\Im}$ but not in both at the same time, where $\vartheta_k^{\Re} = \sum_{i=1}^{u-1} T_{k_i}^{\Re}$ and $\vartheta_k^{\Im} = \sum_{i=1}^{v-1} T_{k_i}^{\Im}$ show the number of decision regions' boundaries according to the following expression

$$\vartheta_k = \begin{cases} \vartheta_k^{\Re}, & \vartheta_k^{\Im} = 0 \\ \vartheta_k^{\Im}, & \vartheta_k^{\Re} = 0 \end{cases}. \tag{8}$$

Therefore, the decision regions' boundaries for the kth bit, $\boldsymbol{d}_k \in \mathbb{R}^{1\times\vartheta_k}$, can be found by considering the indices at which 1 appears, $\boldsymbol{I} \in \mathbb{R}^{1\times\vartheta_k}$, and drawing from the respected primary

decision regions' boundaries basket. This can be written as

$$d_i^{(k)} = \begin{cases} D_{I_i}^{\Re}, & \vartheta_k^{\Im} = 0 \\ D_{I_i}^{\Im}, & \vartheta_k^{\Re} = 0 \end{cases}. \tag{9}$$

Note that $\boldsymbol{d}_k^*$ sorts the $\boldsymbol{d}_k$ elements in a descending order, where this step is important to find the bit error probability as well as the coefficients. The decision boundaries of all NOMA bits for $\boldsymbol{M} = [4, 4, 2]$ can be seen in Fig. 4.

B. Euclidean Distance Computation

As the decision regions' boundaries, $\boldsymbol{d}_k$, for each bit in the NOMA word are found, computing the Euclidean distance between the constellation points is the next step to find the BER expressions. As mentioned previously, due to symmetry, we can consider the first quadrant in the space diagram rather than all transmitted NOMA constellation points. Thus, we are interested in $\boldsymbol{p}^{++}$ which contains the first quadrant elements of the scatter matrix $\boldsymbol{P}$, where $\boldsymbol{p}^{++} \in \mathbb{C}^{1\times 2^{q-2}}$. Therefore, the displacement matrix for the kth bit, $\mathfrak{D}_k$, computes the displacement between the first quadrant constellation points and the decision boundaries. This can be expressed as in (10), where $\mathfrak{D}_k \in \mathbb{R}^{\vartheta_k \times 2^{q-2}}$. Note that each column in $\mathfrak{D}_k$ corresponds to a specific constellation point in $\mathfrak{p}_k^{++}$, while each row corresponds to a specific decision region's boundary in $\boldsymbol{d}_k^*$.

$$\mathfrak{D}_k = \mathfrak{p}_k^{++} - \boldsymbol{d}_k^{*\top} \tag{10}$$

where $^\top$ is the vector transpose, $\mathfrak{D}_k = [\mathfrak{d}_1^{(k)}, \mathfrak{d}_2^{(k)}, \ldots, \mathfrak{d}_{2^{q-2}}^{(k)}]$ and

$$\mathfrak{p}_k^{++} = \begin{cases} \Re[\boldsymbol{p}_k^{++}], & \vartheta_k^{\Im} = 0 \\ \Im[\boldsymbol{p}_k^{++}], & \vartheta_k^{\Re} = 0 \end{cases}. \tag{11}$$

C. Conditional BER Analysis

After studying the conditional BER for different scenarios including the one in Fig. 2, it is noted that the BER mainly depends on the Euclidean distance between the constellation points and the decision regions' boundaries. Therefore, the squared Euclidean distance matrix, $\boldsymbol{E}_k$, can be calculated from $\mathfrak{D}_k$ by squaring all the elements, i.e. $E_{i,j}^{(k)} = \left|\mathfrak{D}_{i,j}^{(k)}\right|^2$. Consequently, the factor that is directly related to the BER expression can be calculated as follows

$$\boldsymbol{\Gamma}_k = \frac{|H_n|^2 \boldsymbol{E}_k}{\sigma_{w_n}^2} \tag{12}$$

where $\mathbf{\Gamma}_k = \left[\boldsymbol{\gamma}_1^{(k)}, \boldsymbol{\gamma}_2^{(k)}, \ldots, \boldsymbol{\gamma}_{\vartheta_k}^{(k)}\right]$, and $\mathrm{SNR} \triangleq 1/\sigma_{W_n}^2$. Note that the user index is dropped for simplicity. Therefore, the conditional BER for each bit is given as

$$P_B^{(k)}|\mathbf{\Gamma}_k = \frac{1}{2^{q-2}} \sum_{i=1}^{\vartheta_k} \sum_{j=1}^{2^{q-2}} c_{i,j}^{(k)} \mathrm{Q}\left(\sqrt{\Gamma_{i,j}^{(k)}}\right) \tag{13}$$

where $\boldsymbol{c}_k = \left[\boldsymbol{c}_1^{(k)}, \boldsymbol{c}_2^{(k)}, \ldots, \boldsymbol{c}_{\vartheta_k}^{(k)}\right]$, $\boldsymbol{c_k} \in \mathbb{R}^{\vartheta_k \times 2^{q-2}}$ turns to a row vector of length 2^{q-2} containing $+1$ elements when $\vartheta_k = 1$, while for $\vartheta_k > 1$, $\boldsymbol{c}_k$ elements can be found according to the following rule

$$c_{i,j}^{(k)} = \begin{cases} (-1)^{i+1}, & G_j^{(k)} = 0 \\ \varphi\left(k, i, j, G_j^{(k)}\right), & G_j^{(k)} > 0 \end{cases} \tag{14}$$

where $G_j^{(k)} = \sum_{i=1}^{\vartheta_k} \psi_{i,j}^k$ and

$$\psi_{i,j}^k = \begin{cases} 1, & \mathfrak{D}_{i,j}^{(k)} < 0 \\ 0, & \mathfrak{D}_{i,j}^{(k)} > 0 \end{cases} \tag{15}$$

and

$$\varphi\left(k, i, j, G_j^{(k)}\right) = \begin{cases} (-1)^{i+1}, & G_j^{(k)} \text{ is odd and } i \leq G_j^{(k)} \\ (-1)^{i}, & G_j^{(k)} \text{ is odd and } i > G_j^{(k)} \\ (-1)^{i}, & G_j^{(k)} \text{ is even and } i \leq G_j^{(k)} \\ (-1)^{i+1}, & G_j^{(k)} \text{ is even and } i > G_j^{(k)} \end{cases} . \tag{16}$$

The expression in (13) considers all the constellation points in the first quadrant of the space diagram. Thus, the weighting factor of $1/2^{q-2}$ is considered as these constellation points are equally probable. Furthermore, each column in $\mathbf{\Gamma}_k$ corresponds to a specific constellation point, where considering the summation over one column would give the probability of error per each constellation point. Note that the rules put to get the coefficients $\boldsymbol{c}_k$ consider the probability that the constellation point falls in an erroneous decision region which corresponds to the BER probability.

To demonstrate (10)–(16), the example shown in Fig. 2 is considered, where the second bit in the NOMA word, b_2, is studied. For brevity, the NOMA word $X = X_e = 01010$ is highlighted. It can be seen that b_2 does not flip if the movement is vertical but it is flipped if the movement

is horizontal. Consequently, the decision regions are alternating horizontally as shown in Fig. 4b. The displacement between the NOMA word X_e and $\boldsymbol{d}_2^*$ can be calculated as follows

$$\begin{aligned}\boldsymbol{\mathfrak{d}}_1^{(2)} &= \mathfrak{p}_1^{(2)^{++}} - \boldsymbol{d}_2^{*\top} \\ &= \left[\mathfrak{D}_{1,1}^{(2)}, \mathfrak{D}_{2,1}^{(2)} \ldots, \mathfrak{D}_{\vartheta_2,1}^{(2)}\right]^\top. \end{aligned} \tag{17}$$

The squared Euclidean distance can be calculated for (17) by squaring the vector elements, i.e. $\boldsymbol{e}_1^{(2)} = \boldsymbol{\mathfrak{d}}_1^{(2)} \cdot \boldsymbol{\mathfrak{d}}_1^{(2)} = \left[E_{1,1}^{(2)}, E_{2,1}^{(2)}, \ldots, E_{\vartheta_2,1}^{(2)}\right]^\top$. Thus, the first column of $\boldsymbol{\Gamma}_k$, (12), can be written as

$$\begin{aligned}\boldsymbol{\gamma}_1^{(2)} &= \frac{|H_1|^2 \boldsymbol{e}_1^{(2)}}{\sigma_{w_1}^2} \\ &= \left[\Gamma_{1,1}^{(2)}, \Gamma_{2,1}^{(2)}, \ldots, \Gamma_{\vartheta_2,1}^{(2)}\right]^\top \end{aligned} \tag{18}$$

Now, the probability that b_2 of the NOMA word X_e can be calculated as follows

$$\begin{aligned}\Pr\left(\widehat{b}_2 \neq b_2 | X = X_e\right) = &\Pr\left(w > \left|\mathfrak{D}_{1,1}^{(2)}\right|\right) + \Pr\left(\left|\mathfrak{D}_{3,1}^{(2)}\right| < w < \left|\mathfrak{D}_{2,1}^{(2)}\right|\right) + \\ &\Pr\left(-\left|\mathfrak{D}_{5,1}^{(2)}\right| < w < -\left|\mathfrak{D}_{4,1}^{(2)}\right|\right) + \\ &\Pr\left(-\left|\mathfrak{D}_{7,1}^{(2)}\right| < w < -\left|\mathfrak{D}_{6,1}^{(2)}\right|\right). \end{aligned} \tag{19}$$

To calculate $\Pr\left(\widehat{b}_2 \neq b_2 | X = X_e\right)$, an integration over the PDF of w must take place. This results in a sum of Gaussian functions, i.e.

$$\begin{aligned}\Pr\left(\widehat{b}_2 \neq b_2 | X = X_e\right) = &c_{1,1}^{(2)} \mathrm{Q}\left(\sqrt{\Gamma_{1,1}^{(2)}}\right) + c_{2,1}^{(2)} \mathrm{Q}\left(\sqrt{\Gamma_{2,1}^{(2)}}\right) + c_{3,1}^{(2)} \mathrm{Q}\left(\sqrt{\Gamma_{3,1}^{(2)}}\right) + \\ &c_{4,1}^{(2)} \mathrm{Q}\left(\sqrt{\Gamma_{4,1}^{(2)}}\right) + c_{5,1}^{(2)} \mathrm{Q}\left(\sqrt{\Gamma_{5,1}^{(2)}}\right) + \\ &c_{6,1}^{(2)} \mathrm{Q}\left(\sqrt{\Gamma_{6,1}^{(2)}}\right) + c_{7,1}^{(2)} \mathrm{Q}\left(\sqrt{\Gamma_{7,1}^{(2)}}\right). \end{aligned} \tag{20}$$

As $G_1^{(2)} = 3$ for this case, the coefficients can be calculated according to (14), where $\boldsymbol{c}_1^{(2)} = [+1, -1, +1, +1, -1, +1, -1]^\top$. Consequently, the conditional BER is calculated for b_2 given that the NOMA word X_e is transmitted. The same steps must be followed for all constellation points in $\mathfrak{p}_k^{++}$ to get the overall conditional BER per bit, (13).

To get the conditional BER per user, each user's bits conditional BER must be averaged. This can be written as

$$P_{B_n} | \boldsymbol{\Gamma}_n = \frac{1}{\log_2 M_n} \sum_{i=O_n}^{O_n + \log_2 M_n} P_B^{(i)} | \boldsymbol{\Gamma}_i \tag{21}$$

where

$$O_n = \begin{cases} 1, & n = 1 \\ 1 + \sum_{i=1}^{n-1} \log_2 M_{n-i}, & n > 1 \end{cases}. \tag{22}$$

D. Unconditional BER Analysis

The conditioning can be eliminated by averaging the conditional BER over the PDF of $\mathbf{\Gamma}_k$ [26], [30]. Thus the unconditional BER per bit over a Rayleigh fading channel can be written as

$$P_B^{(k)} = \frac{1}{2^{q-1}} \sum_{i=1}^{\vartheta_k} \sum_{j=1}^{2^{q-1}} c_{i,j}^{(k)} \zeta \left(\Gamma_{i,j}^{(k)} \right) \tag{23}$$

where $\zeta(\Gamma_{i,j}^{(k)}) = 1 - \sqrt{0.5\overline{\Gamma}_{i,j}^{(k)} \; / \; (1 + 0.5\overline{\Gamma}_{i,j}^{(k)})}$. Similarly, the unconditional BER per user would be the average of each user's bits unconditional BER which is given as follows

$$P_{B_n} = \frac{1}{\log_2 M_n} \sum_{i=O_n}^{O_n + \log_2 M_n} P_B^{(i)}. \tag{24}$$

IV. Power Coefficients Bounds Analysis

The PCBs were introduced in the literature to ensure fairness between users and to avoid the overlap between the NOMA constellation points [15], [25], [27]. Also, PCB ensures the correct placement of each constellation point with respect to other constellation points to avoid constellation points ambiguity problem. In this section, a more generic PCB is introduced for $N = 2$ case [15]. In addition, PCB is analyzed for $N = 3$ case, where arbitrary modulation order is considered at first, then closed-form PCB expressions are shown for NOMA users with identical modulation orders.

A. $N = 2$ Case

The PCB derived in the literature is based on the fact that the nearest constellation point to the origin (NCO) in the first quadrant must not cross over any of the axes. By studying various modulation orders, it turns out that the quadrature axis is the most critical one. Thus, the real part of the NCO needs to be studied. To avoid the NCO crossing over the quadrature axis, the following condition must be satisfied

$$-\frac{\Lambda_1}{\sqrt{\kappa_1}}\sqrt{\alpha_1} + \frac{1}{\sqrt{\kappa_2}}\sqrt{\alpha_2} > 0 \tag{25}$$

TABLE I: Λ_n and κ_n for various modulation orders.

M_n	Λ_n	κ_n
2	1	1
4	1	2
8	3	6
16	3	10
64	7	42

where Λ_n represents the width of the space diagram which is related to M_n, and κ_n is the normalization factor that is used to keep the average power of the user's constellation points as unity, i.e. $E[|x|^2] = 1$. Table I shows Λ_n and κ_n for various modulation orders. The PCB can be derived from (25) and it is given as

$$\frac{\alpha_1}{\alpha_2} < \frac{\kappa_1}{\kappa_2}\frac{1}{\Lambda_1^2} \tag{26}$$

where the maximum possible power coefficient for U_1 can be deduced to be

$$\alpha_{1,\max}^{(N=2)} = \frac{\kappa_1}{\kappa_1 + \kappa_2\Lambda_1^2}. \tag{27}$$

B. $N = 3$ *Case*

To understand the PCB for $N = 3$ case, the superposition coding used to create the final NOMA constellation diagram must be understood. To simplify this, the example in Fig. 2 is studied, where $\boldsymbol{M} = [4, 4, 2]$. The following steps explain the PCB derivation:

1) The first step to have the final NOMA constellation points is to perform superposition coding between U_1 constellation points and U_2 constellation points. The resultant can be seen as the $N = 2$ case which is shown in Fig. 2b. Similarly, the condition in (26) applies here as well, where it can be written as

$$\alpha_2 > \varrho\left(\alpha_1\right) \tag{28}$$

where $\varrho\left(\alpha_1\right) = \frac{\kappa_2}{\kappa_1}\Lambda_1^2\alpha_1$. This can be simplified to

$$\alpha_2 > \alpha_1. \tag{29}$$

2) The second step is to perform superposition coding between the resultant of step 1 and U_3 constellation points. The final NOMA constellation points are shown in Fig. 2c, where

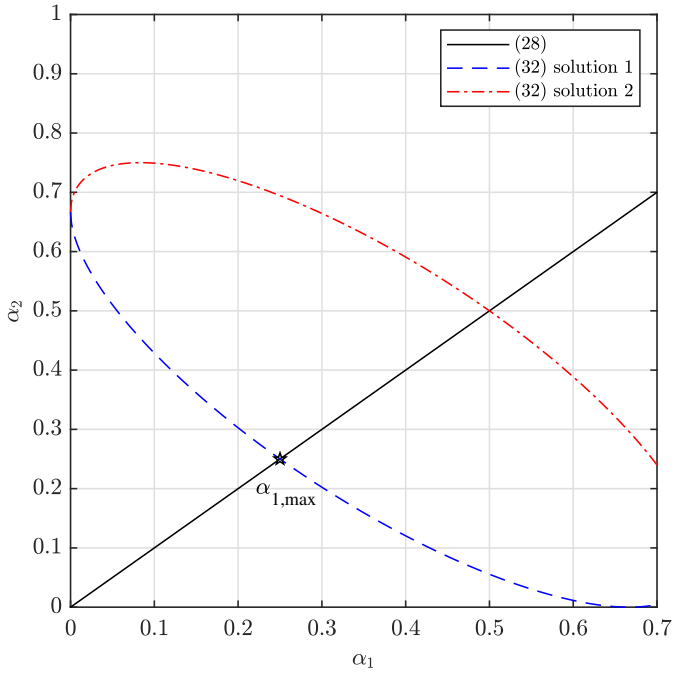

Fig. 5: Visualizing the PCB for $\boldsymbol{M} = [4, 4, 2]$.

it is noted that the NOMA constellation points in Fig. 2b are translated around each constellation point of U_3.

3) Now, the NCO point must not cross over the quadrature axis which represents the worst case scenario. Therefore, the real part of NCO is considered, hence, the condition to be satisfied can be written as

$$-\frac{1}{\sqrt{2}}\sqrt{\alpha_1}-\frac{1}{\sqrt{2}}\sqrt{\alpha_2}+\sqrt{1-\alpha_1-\alpha_2}>0 \tag{30}$$

where this expression can be generalized to arbitrary modulation orders. The generalized form of (30) is

$$-\frac{\Lambda_1}{\sqrt{\kappa_1}}\sqrt{\alpha_1}-\frac{\Lambda_2}{\sqrt{\kappa_2}}\sqrt{\alpha_2}+\frac{1}{\sqrt{\kappa_3}}\sqrt{1-\alpha_1-\alpha_2}>0. \tag{31}$$

4) Solving the inequality in (30) for either α_1 or α_2 results in two solutions in which one of them is not applicable. The solutions of (30) with respect to α_2 are given as

$$\alpha_2 < \varepsilon(\alpha_1) \tag{32}$$

where $\varepsilon(\alpha_1) = -\frac{7}{9}\alpha_1 \mp \frac{2}{9}\sqrt{\alpha_1}\sqrt{-8\alpha_1+6}+\frac{2}{3}$.

5) Fig. 5 visualizes (29) and (32) which makes it easier to infer the PCB. Solution 2 is inapplicable as it leads to NCO crossing over. Hence, it is ignored. However, solution 1

is the desired one, and it needs to be satisfied simultaneously with (29). The intersection between the desired (32) and (29) reflects the maximum possible power coefficient for U_1, $\alpha_{1,\max}$. Therefore, the pair of (α_1, α_2) that satisfies the PCB must be inside the region having the bounds of $\alpha_2 > \alpha_1$ and $\alpha_2 < -\frac{7}{9}\alpha_1 - \frac{2}{9}\sqrt{\alpha_1}\sqrt{-8\alpha_1 + 6} + \frac{2}{3}$.

TABLE II: The PCB for identical modulation orders, $N = 3$

M	$\alpha_{1,\max}$	$\varrho\,(\alpha_1)$	$\varepsilon\,(\alpha_1)$
$[2, 2, 2]$	$\frac{1}{6}$	α_1	$-\sqrt{\alpha_1}\left(\frac{1}{2}\sqrt{\alpha_1} + \frac{1}{2}\sqrt{-3\,\alpha_1 + 2}\right) + \frac{1}{2}$
$[4, 4, 4]$	$\frac{1}{6}$	α_1	$-\sqrt{\alpha_1}\left(\frac{1}{2}\sqrt{\alpha_1} + \frac{1}{2}\sqrt{-3\,\alpha_1 + 2}\right) + \frac{1}{2}$
$[8, 8, 8]$	$\frac{1}{154}$	$9\alpha_1$	$-\frac{9}{5}\sqrt{\alpha_1}\left(-\frac{9}{10}\sqrt{\alpha_1} + \frac{1}{10}\sqrt{-19\,\alpha_1 + 10}\right) - \alpha_1 + \frac{1}{10}$
$[16, 16, 16]$	$\frac{1}{154}$	$9\alpha_1$	$-\frac{9}{5}\sqrt{\alpha_1}\left(-\frac{9}{10}\sqrt{\alpha_1} + \frac{1}{10}\sqrt{-19\,\alpha_1 + 10}\right) - \alpha_1 + \frac{1}{10}$
$[64, 64, 64]$	$\frac{1}{3186}$	$49\alpha_1$	$-\frac{49}{25}\sqrt{\alpha_1}\left(-\frac{49}{50}\sqrt{\alpha_1} + \frac{1}{50}\sqrt{-99\,\alpha_1 + 50}\right) - \alpha_1 + \frac{1}{50}$

By studying various modulation orders, it is noted that the condition in (26) could intersect with the desired solution of the condition in (31) more than once. However, the desired $\alpha_{1,\max}$ is the intersection that gives the minimum value of α_1. Furthermore, Table II summarizes the PCB for the identical modulation schemes, where the trend can be inferred. Consequently, closed-form expressions for the PCB are shown in (33) and (34), where $\varpi = \Lambda_1^2 + 1$, $\lceil . \rceil$ and $\lfloor . \rfloor$ are the ceil and floor operations.

$$\alpha_{1,\max}^{(N=3)} = \left(\varpi + M_1(\varpi - 1) \times 2^{\left\lfloor \frac{\log_2(M_1) - (-1)^{\log_2(M_1)}}{M_1} + \frac{1}{2} \right\rfloor}\right)^{-1} \tag{33}$$

$$\varepsilon\,(\alpha_1) = \tfrac{1}{\varpi} - \tfrac{2(\varpi-1)}{\varpi}\sqrt{\alpha_1}\left(\tfrac{\varpi-1}{\varpi}\sqrt{\alpha_1} \times (-1)^{\left\lfloor \frac{\log_2(M_1)}{M_1} + 0.5 \right\rfloor} + \tfrac{1}{\varpi}\sqrt{\varpi - (2\varpi - 1)\alpha_1}\right) - \alpha_1 \times \left\lceil \left| \tfrac{\log_2(M_1)}{M_1} - 0.5 \right| \right\rceil \tag{34}$$

The closed-form PCB expressions can be used as linear and non-linear constraints to solve minimization or maximization optimization problems. For instance, given that the average BER of the two users NOMA system, i.e. system's average BER, is $P_{B,\text{Avg.}}^{(N=2)} = 0.5 \times (P_{B_1} + P_{B_2})$, then the optimization problem to find the optimal power assignment that minimizes the system's average BER is formulated as

$$\begin{aligned} \underset{\boldsymbol{\alpha}}{\text{minimize}} \quad & P_{B,\text{Avg.}}^{(N=2)} \\ \text{subject to} \quad & \alpha_1 < \alpha_{1,\max}^{(N=2)}, \\ & \alpha_1 + \alpha_2 = 1 \end{aligned} \tag{35}$$

where the inequality constraint, which satisfies the PCB condition, is linear for $N = 2$ case. The equality constraint is considered to ensure that the transmitted power is normalized to unity. The objective function is non-linear and according to [22], the non-linear optimization results in a near optimum solution. Similarly, the optimization problem can be extended to three users case, where $P_{B,\text{Avg.}}^{(N=3)} = \frac{1}{3} \times (P_{B_1} + P_{B_2} + P_{B_3})$. As such, the optimization problem is formulated as

$$\begin{aligned} \underset{\boldsymbol{\alpha}}{\text{minimize}} \quad & P_{B,\text{Avg.}}^{(N=3)} \\ \text{subject to} \quad & \alpha_1 < \alpha_{1,\max}^{(N=3)}, \\ & \varrho\left(\alpha_1\right) < \alpha_2 < \varepsilon(\alpha_1), \\ & \alpha_1 + \alpha_2 + \alpha_3 = 1 \end{aligned} \tag{36}$$

where the first inequality constraint is linear, and it is similar to $N = 2$ case. However, one more inequality constraint is introduced, where its upper bound is non-linear, whereas the lower bound is linear. The equality constraint is similar to $N = 2$ case.

V. Numerical Results and Discussions

This section presents the BER results of a downlink C-NOMA system using arbitrary modulation orders. The BER is computed analytically using the expressions in Sec. III and validated by Monte Carlo simulations. In addition, the optimal power assignments that minimize the system's average BER for $N = 2$ and 3 cases are found, where the PCBs derived in Sec. IV are used as constraints to solve the non-linear optimization problem using interior point optimization (IPO) algorithm [22]. It is worth noting that the PCB constraints increased from one constraint for $N = 2$, to three constraints for $N = 3$. Moreover, the small scale fading is considered as a flat Rayleigh random variable with $\sigma_{h_n}^2 = 1$, and the large scale fading is considered as fixed pathloss with an exponent of $\lambda = 2.7$, where the users are at a distance of $\Upsilon_n = 10^{\frac{3}{5\lambda}(n-1)}$ from the base station. Also, σ_{W_n} is assumed to be a common factor for all users which means that $\text{SNR} \triangleq 1/\sigma_W^2$, thus it is common as well. It is important to note that the SNR does not reflect the effective SNR, SNR_{eff}, at the receiver because the power coefficient and the pathloss coefficient are not factored in. This is a common practice in the literature because it allows having a common x-axis for all users which is useful for direct comparisons [15], [20]–[22], [26]. The base station and all users are assumed to be equipped with a single antenna. Moreover, the power assignment for $N = 2$ is selected to satisfy (26) for all considered modulation orders jointly, where the worst case scenario is when $\boldsymbol{M} = [8, 64]$. Hence, $\alpha_1 = 0.01$ and $\alpha_2 = 0.99$.

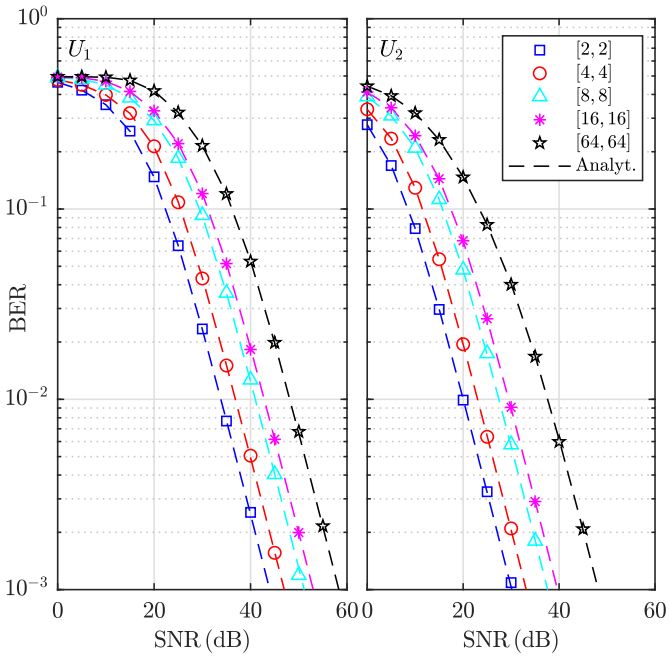

Fig. 6: Simulation and analytical results for the unconditional BER, where $N = 2$, and $M_1 = M_2$.

Similarly, when $N = 3$, the power assignment needs to satisfy (28) and (32) simultaneously for all considered modulation orders. Thus, the selected power assignment is $\alpha_1 = 0.0001$, $\alpha_2 = 0.01$ and $\alpha_3 = 0.9899$. The legends in the figures, where $2 \leq N \leq 4$ represent the modulation order vectors, $\boldsymbol{M}$. Furthermore, for $N > 3$ cases, brute force technique is used to select the proper power assignments.

Fig. 6 shows the analytical and simulation results of the unconditional BER for $N = 2$ case with identical modulation orders. The figure shows exact match between analytical and simulation results. It is noted that as the modulation order goes higher, the BER performance degrades for both users. For instance, QPSK modulation for both users requires roughly 3 dB more than BPSK to get a BER of 10^{-2}. For this power assignment, the 3 dB figure is similar to the difference between BPSK and QPSK for the single user system. Moreover, when comparing BPSK and 64-QAM, the latter requires a boost of 14.36 and 17.54 dB for U_1 and U_2 to get the 10^{-2} BER.

The BER results shown in Fig. 7 are for U_1 and U_2, where the modulation orders are not necessarily identical. It is noted that at high SNR values each user's BER is almost independent of the other user's modulation order except for the case of $\boldsymbol{M} = [8, 64]$. This is justified by

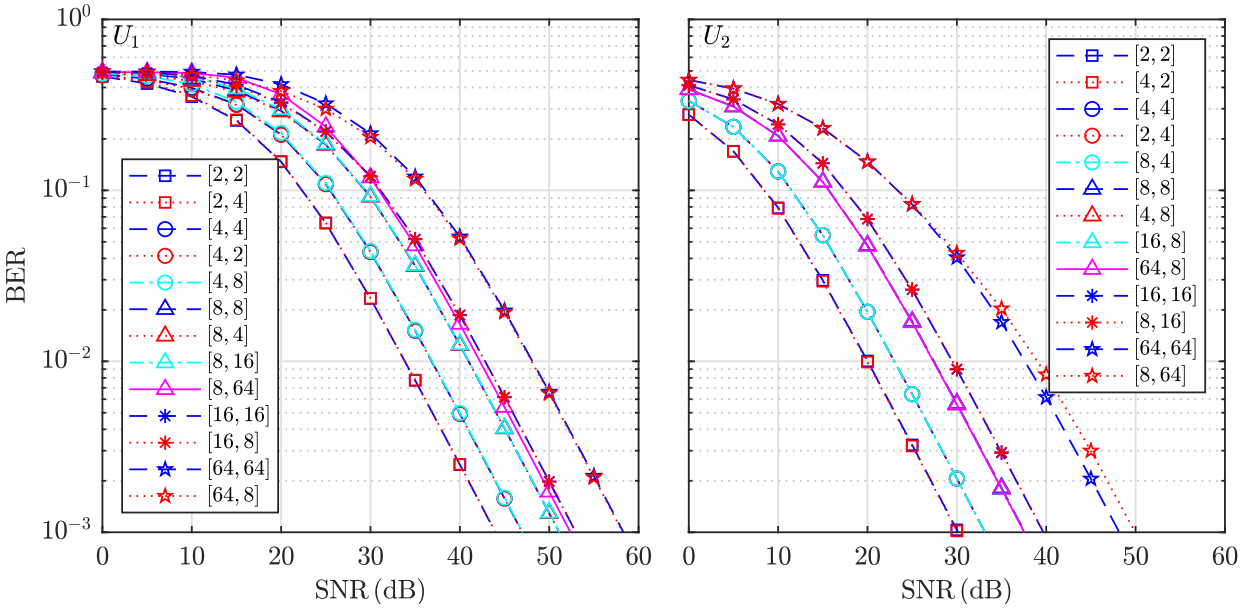

Fig. 7: U_1 and U_2 unconditional BER for various modulation schemes, where $N = 2$.

the fact that the selected power assignment is close to the PCB (26). However, for the rest of modulation orders combinations, the selected power assignments are relatively far from the PCB. Fig. 8 shows the percentage of change of the BER relative to the identical modulation order case. For instance, the BER percentage of change for U_1 with $\boldsymbol{M} = [8, 4]$ is calculated with $\boldsymbol{M} = [8, 8]$ as a reference. However, for U_2 with $\boldsymbol{M} = [8, 4]$, the percentage of change is calculated with $\boldsymbol{M} = [4, 4]$ as a reference. It is noted that the percentage of change stabilizes at high SNR values. For instance, for U_1 it peaks before stabilization, however, for U_2 the stabilization is a plateau. In addition, the percentage of change for U_1 at high SNR values is within $\pm 2\%$ for all modulation orders, except $\boldsymbol{M} = [8, 64]$ which plateaus with a percentage of change of $+30\%$. Similarly, the percentage of change for U_2 is within $\pm 2\%$, except for $\boldsymbol{M} = [8, 64]$ which plateaus with a percentage of change of $+50\%$. Furthermore, the optimal power assignment that minimizes the two users average BER, i.e. $0.5 \times (P_{B_1} + P_{B_2})$, is summarized in Table III in the Appendix including the achieved average BER at such power assignments, where various SNR conditions are considered. It can be seen that the optimal power assignments for a given modulation order are roughly changed at high SNR values.

The unconditional BER results for various modulation orders when $N = 3$ are shown in Fig. 9. A similar trend to the $N = 2$ case is observed here as well, where the BER performance

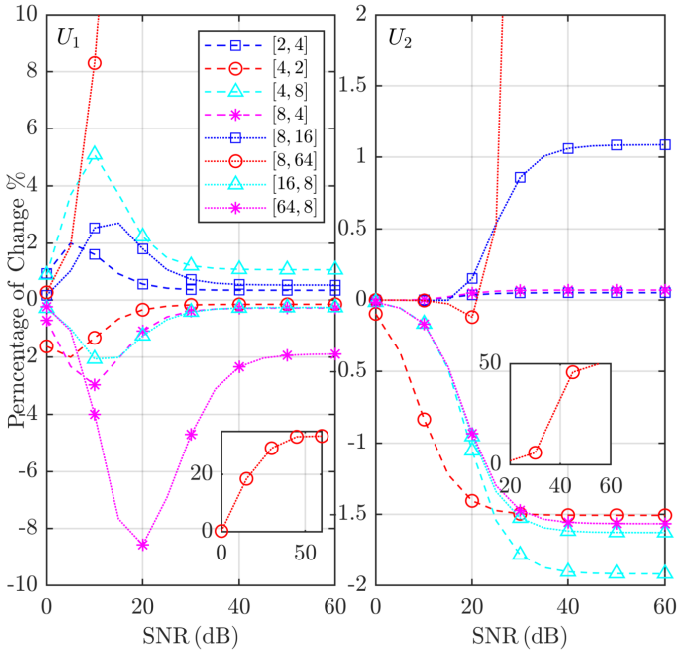

Fig. 8: The BER percentage of change w.r.t. the identical modulation case, $N = 2$.

gets worse when higher modulation order is selected. However, the overall BER performance is degraded compared to $N = 2$. For instance, considering the identical BPSK case, U_3 which is given the highest power coefficient, requires 26 dB to get a BER of 10^{-2}, whereas U_2 in $N = 2$ case, the highest power user, requires 20 dB to get the same BER. Similarly, when comparing U_2 in $N = 3$ case with U_1 in $N = 2$ case, it is noted that the former requires 6.14 dB more to achieve the BER threshold even though both users are given the same power coefficient. This is justified by the fact that as the number of users increases, the IUI increases as well leading to a performance loss. Moreover, considering the identical BPSK scenario as a benchmark, the identical QPSK scenario requires 3.05, 3.1, and 2.92 dB more for U_1, U_2 and U_3 to reach to the BER threshold of 10^{-2}. Similarly, the 16-QAM scenario requires 9, 9.56, and 9.45 dB more for U_1, U_2 and U_3 to get the same BER threshold. Furthermore, it is noted that at high SNR values, the BER performance for each user is almost independent of the other users' modulation orders when the selected power assignment is far away from the PCB, which is the case here. Fig. 10 shows the percentage of change of the BER relative to the identical modulation order case, where it can be seen that U_1 and U_2 follow the same trend for U_1 in $N = 2$ case, while U_3 follows the trend of U_2 in $N = 2$. The reason is that the power coefficients of U_1 and U_2

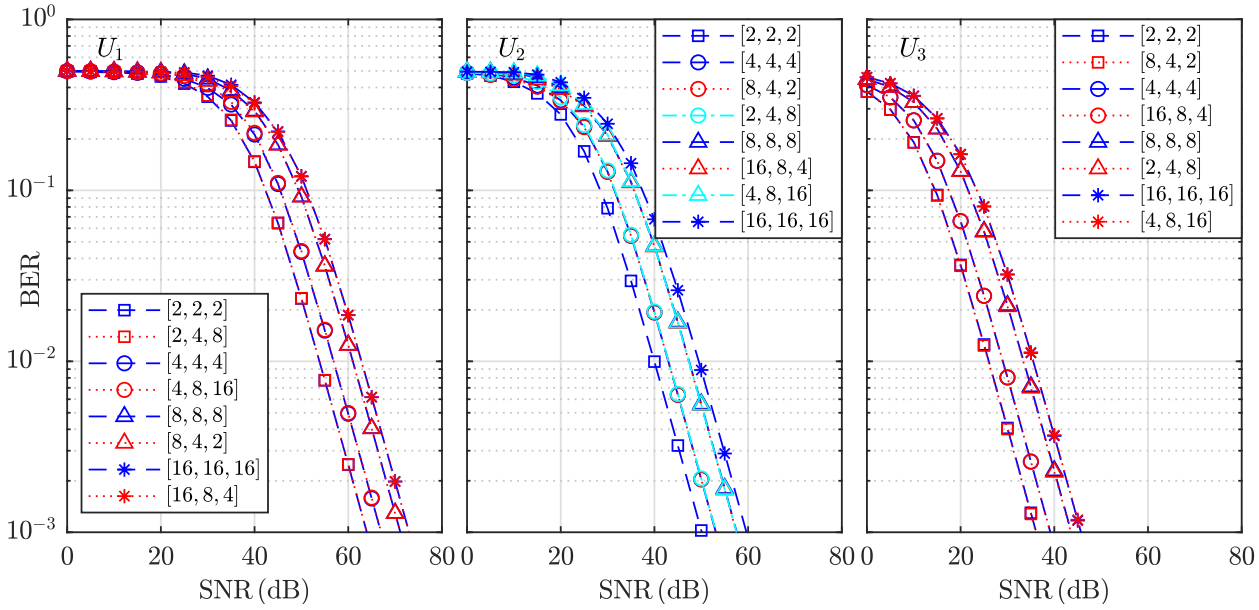

Fig. 9: Unconditional BER for various modulation schemes, where $N = 3$.

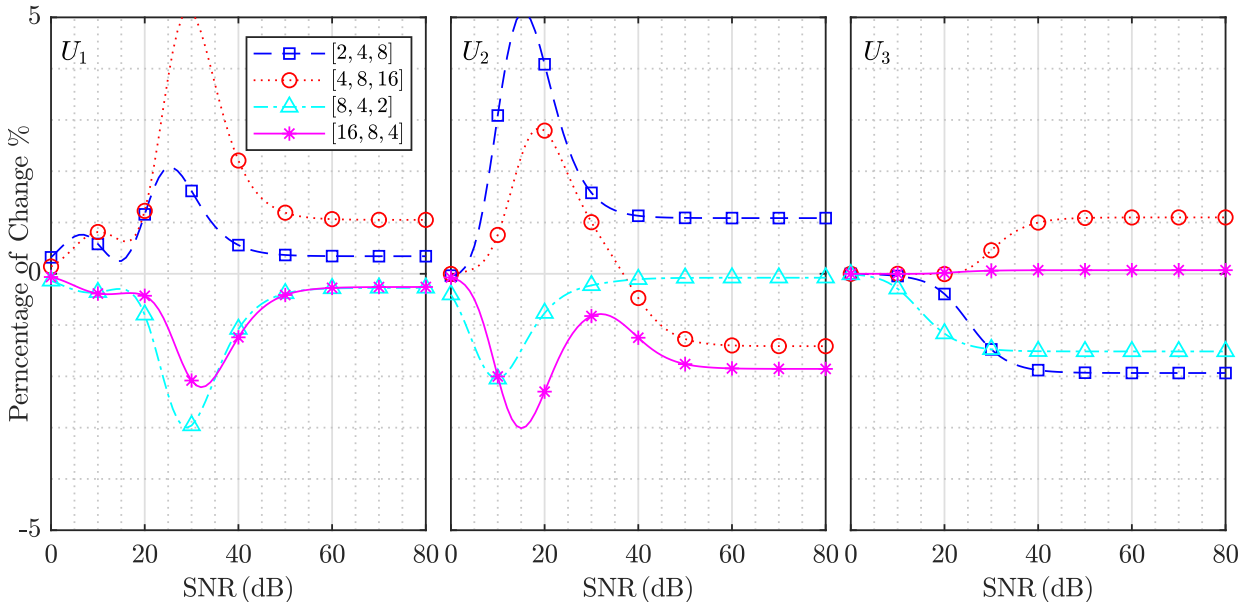

Fig. 10: The BER percentage of change w.r.t. the identical modulation case, $N = 3$.

are relative to U_1 in $N = 2$, whereas the power coefficient of U_3 is relative to U_2 in $N = 2$. In addition, the percentage of changes at high SNR values are roughly within $\pm 1\%$, $\pm 2\%$ and $\pm 2\%$ for U_1, U_2 and U_3 respectively.

The optimal power assignment which minimizes the users' average BER for $N = 3$ case,

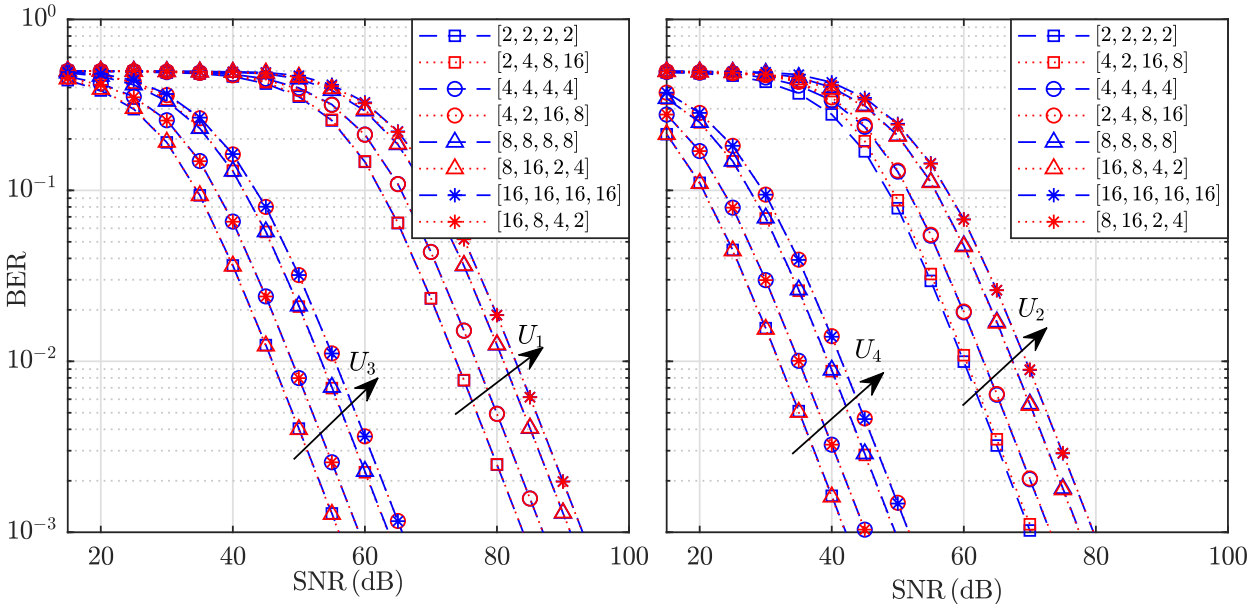

Fig. 11: Unconditional BER for various modulation schemes, where $N = 4$.

i.e. $\frac{1}{3} \times (P_{B_1} + P_{B_2} + P_{B_3})$, is shown for various SNR conditions in Table IV in the Appendix. Similar to the $N = 2$ case, the optimal power assignment is roughly changed for high SNR values. In addition, it can be seen that as the SNR conditions improve for U_1, portion of its power is given to other users with higher pathloss. This can be understood by the fact that the users' average BER is dominated by the worst case BER, hence, improving it would improve the average BER.

The four users case is considered in Fig. 11, where it shows the unconditional BER given that the power assignment is found via brute force to satisfy the PCBs for various considered modulation orders. The power assignment is found to be $\alpha_1 = 0.000001$, $\alpha_2 = 0.0001$, $\alpha_3 = 0.01$ and $\alpha_4 = 0.989899$, which requires very fine control at the base station to achieve the required sensitivity. The fact that each user's BER is independent of other users' modulation orders is confirmed here as well. Nonetheless, it is noted that the overall BER performance is degraded compared to lower number of users because the near users are given a very small fraction in order to have a proper positioning of the NOMA constellation points. Another reason is the user distance model used in which the pathloss increases as the user's index increases. For instance, the experienced pathloss by the furthest user is 24 dB. Furthermore, considering the worst case which is the identical 16-QAM as a benchmark and setting the BER threshold to 10^{-2}, U_2 in

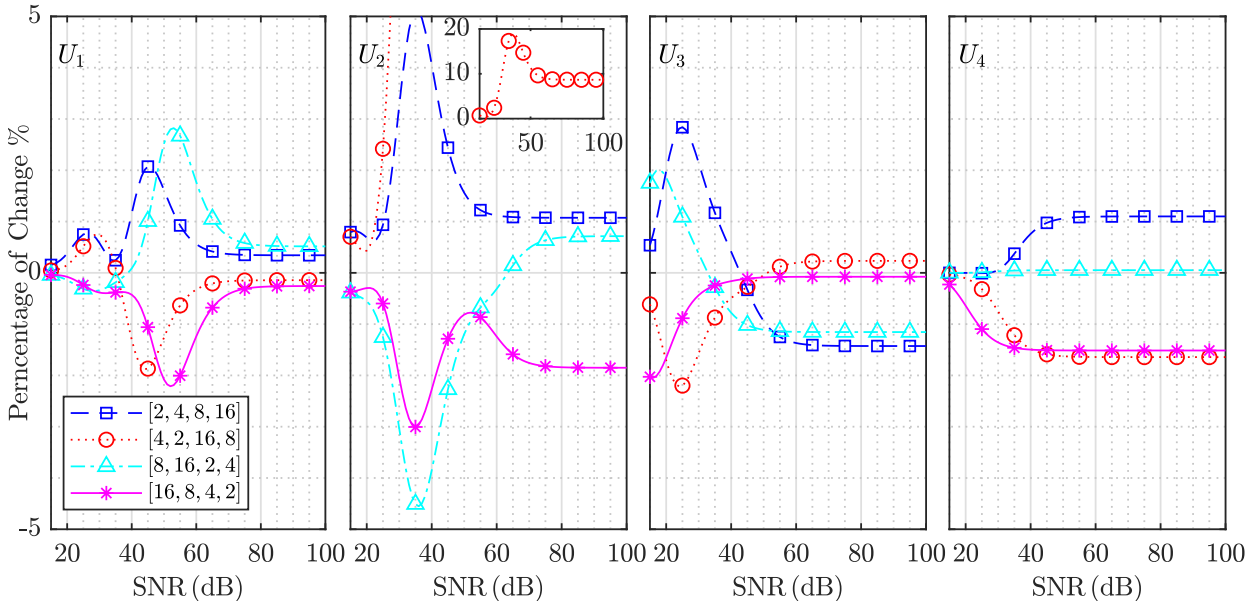

Fig. 12: The BER percentage of change w.r.t. the identical modulation case, $N = 4$.

$N = 4$ loses 7.5 dB compared to U_1 in $N = 3$ case even though both have identical power coefficients. Similarly, U_3 in $N = 3$ case loses 6 dB compared to U_2 in $N = 3$ case having said that both have identical power coefficients. Again, it can be seen that the BER of each user is almost independent of the other users' modulation orders at high SNR values. However, the performance is not identical for such cases which is confirmed by Fig. 12, where the percentage of change of the BER with respect to the identical modulation order is shown. It is noted that the first three users have the same trend as U_1 in $N = 2$ case, whereas the furthest user follows the trend of U_2 in $N = 2$ case. It can be seen that the percentage of change at high SNR values is within $\pm 0.5\%$, $\pm 2\%$, $\pm 1\%$ and $\pm 2\%$ for U_1–U_4 except the modulation order of $\boldsymbol{M} = [4, 2, 16, 8]$ for U_2 which plateaus with a percentage of change of $+10\%$.

Finally, Fig. 13 shows the BER for arbitrary number of users using identical QPSK modulation orders. The selected power assignment for each case is found by brute force, where proper constellation points positioning is ensured as well as minimum system's average BER. The power assignment, $\{\alpha_1, \alpha_2, \ldots, \alpha_N\}$, is:

- $N = 2$: $\{0.1382,\ 0.8618\}$
- $N = 3$: $\{0.0232,\ 0.1559,\ 0.8209\}$
- $N = 4$: $\{0.0044,\ 0.0296,\ 0.1645,\ 0.8016\}$

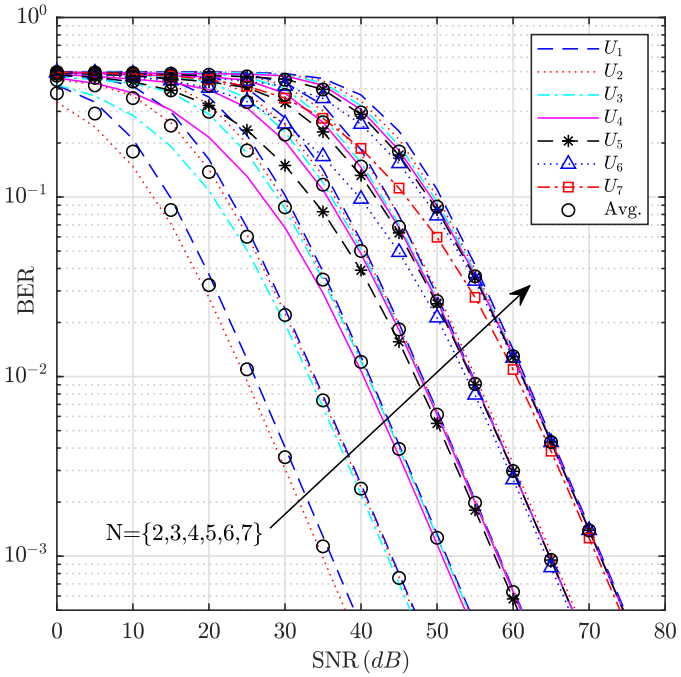

Fig. 13: Unconditional BER for various number of users cases, where $M_1 = M_2 = \ldots = M_N = 4$.

- $N = 5$: $\{0.0009,\ 0.0059,\ 0.0333,\ 0.1695,\ 0.7904\}$
- $N = 6$: $\{0.0002,\ 0.0012,\ 0.0070,\ 0.0357,\ 0.1728,\ 0.7831\}$
- $N = 7$: $\{3.9940 \times 10^{-5},\ 2.6892 \times 10^{-4},\ 0.0015,\ 0.0077,\ 0.0375,\ 0.1752,\ 0.7778\}$

It is noted that at high SNR values the BER of all users converge very closely to the average BER, where the channel difference between the users is negligible at such SNR conditions. It is also confirmed that there is a trade-off between N and the BER performance, where the overall BER performance is degraded as N increases. By considering the average BER of the $N = 2$ case as a benchmark and the BER threshold as 10^{-3}, it is noted that an SNR boost between 6.65 and 8.24 dB is required to achieve the BER threshold if N increases with a step of 1.

VI. Conclusions

To conclude, this paper derived exact analytical BER expressions for C-NOMA over Rayleigh flat fading channels, where the expressions are generalized for any number of users, N, and any arbitrary modulation order. These expressions were verified by Monte Carlo simulations in which the analytical and the simulation results were perfectly matched. It was also demonstrated that

there is a trade-off between N and the overall BER performance, where as the former increases, the latter degrades. In addition, it was revealed that the BER of all users tend to converge closely to the average BER at high SNR values. Moreover, the conclusion in [15] is confirmed for $N = 3$ case as well, where the BER of each user is independent from other users' modulation orders if the power assignment is far away from the PCB. Furthermore, the steps to get the PCB for $N = 3$ were presented and closed-form expressions were shown for the identical modulation order case. These expressions were used as linear and non-linear constraints to find optimal power assignment that minimizes the average BER for $N = 2$ and $N = 3$ cases.

APPENDIX
OPTIMAL POWER ASSIGNMENTS

The optimal power assignments to minimize the system's average BER are listed in Table III and Table IV for $N = 2$ and $N = 3$ cases considering different modulation orders and SNR conditions.

TABLE III: Optimal power assignment including the average BER for different modulation schemes under various SNR conditions, $N = 2$.

	15 dB		30 dB		45 dB		60 dB	
$\boldsymbol{M}$	α_1	BER	α_1	BER	α_1	BER	α_1	BER
$[2, 2]$	0.145	5.3E−2	0.138	2.0E−3	0.138	6.3E−5	0.138	2.0E−6
$[4, 4]$	0.151	9.1E−2	0.139	4.0E−3	0.138	1.3E−4	0.138	4.0E−6
$[8, 8]$	0.062	2.1E−1	0.052	1.9E−2	0.050	6.5E−4	0.050	2.1E−5
$[16, 16]$	0.052	2.5E−1	0.047	3.0E−2	0.046	1.1E−3	0.046	3.5E−5
$[64, 64]$	0.011	3.5E−1	0.013	1.2E−1	0.013	9.7E−3	0.013	3.3E−4
$[4, 2]$	0.244	5.6E−2	0.232	2.2E−3	0.232	6.9E−5	0.232	2.2E−6
$[2, 4]$	0.103	7.9E−2	0.092	3.3E−3	0.092	1.9E−4	0.092	3.3E−6
$[8, 4]$	0.154	1.3E−1	0.136	7.3E−3	0.135	2.4E−4	0.135	7.6E−6
$[4, 8]$	0.070	1.7E−1	0.057	9.9E−3	0.057	3.2E−4	0.057	1.0E−5
$[16, 8]$	0.082	2.1E−1	0.073	2.0E−2	0.072	7.0E−4	0.072	2.2E−5
$[8, 16]$	0.042	2.4E−1	0.034	2.8E−2	0.032	1.0E−3	0.032	3.2E−5
$[64, 8]$	0.079	2.4E−1	0.082	4.1E−2	0.082	1.7E−3	0.082	5.4E−5
$[8, 64]$	0.011	3.4E−1	0.009	8.0E−2	0.008	3.8E−3	0.008	1.2E−4

TABLE IV: Optimal power assignment including the average BER for different modulation schemes under various SNR conditions, $N = 3$.

	15 dB			30 dB			45 dB			60 dB		
$\boldsymbol{M}$	α_1	α_2	BER	α_1	α_2	BER	α_1	α_2	BER	α_1	α_2	BER
$[2, 2, 2]$	0.032	0.180	1.8E−1	0.024	0.158	1.2E−2	0.023	0.156	3.8E−4	0.024	0.160	1.2E−5
$[4, 4, 4]$	0.035	0.187	2.5E−1	0.024	0.160	2.2E−2	0.023	0.156	7.6E−4	0.023	0.156	2.4E−5
$[8, 8, 8]$	0.004	0.066	3.8E−1	0.003	0.059	1.2E−1	0.003	0.055	8.5E−3	0.003	0.054	2.8E−4
$[16, 16, 16]$	0.003	0.038	4.1E−1	0.003	0.056	1.7E−1	0.003	0.054	1.5E−2	0.002	0.054	5.0E−4
$[8, 4, 2]$	0.049	0.289	2.1E−1	0.040	0.263	2.1E−2	0.038	0.261	7.2E−4	0.038	0.262	2.3E−5
$[2, 4, 8]$	0.009	0.096	3.3E−1	0.006	0.067	4.6E−2	0.005	0.127	3.8E−3	0.006	0.064	5.5E−5
$[16, 8, 4]$	0.017	0.175	3.1E−1	0.013	0.158	6.8E−2	0.011	0.149	3.4E−3	0.011	0.148	1.1E−4
$[4, 8, 16]$	0.007	0.022	3.9E−1	0.003	0.039	1.3E−1	0.002	0.035	7.3E−3	0.002	0.035	2.4E−4

REFERENCES

[1] Z. Zhang, Y. Xiao, Z. Ma, M. Xiao, Z. Ding, X. Lei, G. K. Karagiannidis, and P. Fan, "6G wireless networks: Vision, requirements, architecture, and key technologies," *IEEE Veh. Technol Mag.*, vol. 14, no. 3, pp. 28–41, Sep. 2019.

[2] M. Vaezi, R. Schober, Z. Ding, and H. V. Poor, "Non-orthogonal multiple access: Common myths and critical questions," *IEEE Wireless Commun.*, vol. 26, no. 5, pp. 174–180, Oct. 2019.

[3] O. Maraqa, A. S. Rajasekaran, S. Al-Ahmadi, H. Yanikomeroglu, and S. M. Sait, "A survey of rate-optimal power domain NOMA with enabling technologies of future wireless networks," *IEEE Commun. Surveys Tuts.*, pp. 1–1, Aug. 2020.

[4] L. Dai, B. Wang, Z. Ding, Z. Wang, S. Chen, and L. Hanzo, "A survey of non-orthogonal multiple access for 5G," *IEEE Commun. Surveys Tuts.*, vol. 20, no. 3, pp. 2294–2323, May 2018.

[5] Y. Liu, Z. Qin, M. Elkashlan, Z. Ding, A. Nallanathan, and L. Hanzo, "Nonorthogonal multiple access for 5G and beyond," *Proc. IEEE*, vol. 105, no. 12, pp. 2347–2381, Dec. 2017.

[6] M. Shirvanimoghaddam *et al.*, "Massive non-orthogonal multiple access for cellular IoT: Potentials and limitations," *IEEE Commun. Mag.*, vol. 55, no. 9, pp. 55–61, Sep. 2017.

[7] Z. Xiang, W. Yang, Y. Cai, Z. Ding, Y. Song, and Y. Zou, "NOMA-assisted secure short-packet communications in IoT," *IEEE Wireless Commun.*, vol. 27, no. 4, pp. 8–15, Aug. 2020.

[8] A. I. Perez-Neira, M. Caus, and M. A. Vazquez, "Non-orthogonal transmission techniques for multibeam satellite systems," *IEEE Commun. Mag.*, vol. 57, no. 12, pp. 58–63, Dec 2019.

[9] X. Zhu, C. Jiang, L. Kuang, N. Ge, S. Guo, and J. Lu, "Cooperative transmission in integrated terrestrial-satellite networks," *IEEE Netw.*, vol. 33, no. 3, pp. 204–210, May/Jun. 2019.

[10] Y. Liu, Z. Qin, Y. Cai, Y. Gao, G. Y. Li, and A. Nallanathan, "UAV communications based on non-orthogonal multiple access," *IEEE Wireless Commun.*, vol. 26, no. 1, pp. 52–57, Feb. 2019.

[11] H. Marshoud, S. Muhaidat, P. C. Sofotasios, S. Hussain, M. A. Imran, and B. S. Sharif, "Optical non-orthogonal multiple access for visible light communication," *IEEE Wireless Commun.*, vol. 25, no. 2, pp. 82–88, Apr. 2018.

[12] M. Jain, N. Sharma, A. Gupta, D. Rawal, and P. Garg, "Performance analysis of NOMA assisted underwater visible light communication system," *IEEE Wireless Commun. Lett.*, vol. 9, no. 8, pp. 1291–1294, Aug. 2020.

[13] Y. Saito, Y. Kishiyama, A. Benjebbour, T. Nakamura, A. Li, and K. Higuchi, "Non-orthogonal multiple access (NOMA) for cellular future radio access," in *Proc. IEEE Veh. Technol. Conf. (VTC Spring)*, Dresden, Germany, Jun. 2013, pp. 1–5.

[14] N. I. Miridakis and D. D. Vergados, "A survey on the successive interference cancellation performance for single-antenna and multiple-antenna OFDM systems," *IEEE Commun. Surveys Tuts.*, vol. 15, no. 1, pp. 312–335, 1st Quart. 2013.

[15] T. Assaf, A. Al-Dweik, M. S. El Moursi, H. Zeineldin, and M. Al-Jarrah, "Exact bit error-rate analysis of two-user NOMA using QAM with arbitrary modulation orders," *IEEE Commun. Lett.*, pp. 1–1, Sep. 2020.

[16] T. Assaf, A. Al-Dweik, M. S. E. Moursi, H. Zeineldin, and M. Al-Jarrah, "NOMA receiver design for delay-sensitive systems," *IEEE Syst. J.*, pp. 1–12, 2020.

[17] E. C. Cejudo, H. Zhu, and O. Alluhaibi, "On the power allocation and constellation selection in downlink NOMA," in *Proc. IEEE Veh. Technol. Conf. (VTC Fall)*, Toronto, ON, Canada, Sep. 2017, pp. 1–5.

[18] X. Wang, F. Labeau, and L. Mei, "Closed-form BER expressions of QPSK constellation for uplink non-orthogonal multiple access," *IEEE Commun. Lett.*, vol. 21, no. 10, pp. 2242–2245, Oct. 2017.

[19] H. Marshoud, P. C. Sofotasios, S. Muhaidat, G. K. Karagiannidis, and B. S. Sharif, "On the performance of visible light communication systems with non-orthogonal multiple access," *IEEE Trans. Wireless Commun.*, vol. 16, no. 10, pp. 6350–6364, Oct. 2017.

[20] F. Kara and H. Kaya, "BER performances of downlink and uplink NOMA in the presence of SIC errors over fading channels," *IET Commun.*, vol. 12, no. 15, pp. 1834–1844, Sep. 2018.

[21] L. Bariah, S. Muhaidat, and A. Al-Dweik, "Error probability analysis of non-orthogonal multiple access over Nakagami-m fading channels," *IEEE Trans. Commun.*, vol. 67, no. 2, pp. 1586–1599, Feb. 2019.

[22] T. Assaf, A. Al-Dweik, M. E. Moursi, and H. Zeineldin, "Exact BER performance analysis for downlink NOMA systems over Nakagami-m fading channels," *IEEE Access*, vol. 7, pp. 134 539–134 555, Sep. 2019.

[23] X. Liu, Z. Chen, Y. Wang, F. Zhou, Y. Luo, and R. Q. Hu, "BER analysis of NOMA-enabled visible light communication systems with different modulations," *IEEE Trans. Veh. Technol.*, vol. 68, no. 11, pp. 10 807–10 821, Nov. 2019.

[24] A. S. Alqahtani and E. Alsusa, "Performance analysis of downlink NOMA system over α-η-μ generalized fading channel," in *Proc. IEEE Veh. Technol. Conf. (VTC Spring)*, Antwerp, Belgium, May 2020, pp. 1–5.

[25] M. Aldababsa, C. Göztepe, G. K. Kurt, and O. Kucur, "Bit error rate for NOMA network," *IEEE Commun. Lett.*, vol. 24, no. 6, pp. 1188–1191, Mar. 2020.

[26] H. Yahya, A. Dweik, and E. Alsusa, "Power-tolerant NOMA using data-aware adaptive power assignment for IoT systems," *submitted to IEEE IoT. J.*, Aug. 2020.

[27] I. Lee and J. Kim, "Average symbol error rate analysis for non-orthogonal multiple access with M-ary QAM signals in Rayleigh fading channels," *IEEE Commun. Lett.*, vol. 23, no. 8, pp. 1328–1331, Jun. 2019.

[28] H. Xu and N. Pillay, "Threshold based signal detection and the average symbol error probability for downlink NOMA systems with M-ary QAM," *IEEE Access*, vol. 8, pp. 156 677–156 685, Aug. 2020.

[29] Q. He, Y. Hu, and A. Schmeink, "Closed-form symbol error rate expressions for non-orthogonal multiple access systems," *IEEE Trans. Veh. Technol.*, vol. 68, no. 7, pp. 6775–6789, May 2019.

[30] M. Simon and M. Alouini, *Digital Communication Over Fading Channels*, 2nd ed. Hoboken, New Jersey, USA: Wiley-Interscience, 2005.